FILIPPINI, G., GRAMACCIOLI, M., SIMONETTA, M. & SUFFRITTI, G. B. (1973). *J. Chem. Phys.* **59**, 5088-5101.
FILIPPINI, G., GRAMACCIOLI, M., SIMONETTA, M. & SUFFRITTI, G. B. (1975). *Chem. Phys.* **8**, 136-146.
HSU, L. Y. & WILLIAMS, D. E. (1980). *Acta Cryst.* A**36**, 277-281.
JINDAL, V. K. & KALUS, J. (1983). *J. Phys. C*, **16**, 3061-3080.
KITAIGORODSKII, A. I. (1969). *Sov. Phys. Crystallogr.* **14**, 769-774.
KITAIGORODSKII, A. I. (1973). *Molecular Crystals and Molecules.* New York: Academic Press.
KROON, P. & VOS, A. (1978). *Acta Cryst.* A**34**, 823-824.
MIRSKAYA, K. V. & NAUCHITEL, V. V. (1971). *Sov. Phys. Crystallogr.* **16**, 891-892.
MIRSKAYA, K. V. & NAUCHITEL, V. V. (1972). *Sov. Phys. Crystallogr.* **17**, 56-59.
SCHOMAKER, V. & TRUEBLOOD, K. N. (1968). *Acta Cryst.* B**24**, 63-76.
WILLIAMS, D. E. (1967). *J. Chem. Phys.* **47**, 4680-4684.
WILLIAMS, D. E. (1971). *Acta Cryst.* A**27**, 452-455.
WILLIAMS, D. E. (1974). *Acta Cryst.* A**30**, 71-77.
WILLIAMS, D. E. & COX, S. R. (1984). *Acta Cryst.* B**40**, 404-417.
WILLIS, B. T. & PRYOR, A. W. (1975). *Thermal Vibrations in Crystallography.* Cambridge Univ. Press.

Acta Cryst. (1986). B**42**, 613-621

Hydrogen Bonding and Thermal Vibrations in Crystalline Phosphate Salts of Histidine and Imidazole

BY ROBERT H. BLESSING

Medical Foundation of Buffalo, Inc., 73 High Street, Buffalo, New York 14203, *USA*

(*Received* 19 *February* 1986; *accepted* 30 *June* 1986)

Abstract

Salts of composition $Im.H_3PO_4$ and L-$His.2H_3PO_4$ were prepared and analyzed by X-ray crystallography. The Im salt forms a rather complicated crystal structure with two chemical formula units in the crystal chemical unit and the crystals of the His salt contain unionized molecular H_3PO_4. There are networks of short strong hydrogen bonds in both crystals, and the hydrogen bonding noticeably affects the O-atom thermal vibrations. The hydrogen-bonding geometries indicate that N–H···O–P and P–O–H···O–P bonds are generally the strongest N–H···O and O–H···O bonds that can form in biochemical systems, and the strong hydrogen bonding significantly affects the P–O bond strengths. Crystal data: L-histidinium dihydrogen orthophosphate orthophosporic acid, $C_6H_{10}N_3O_2^+.H_2PO_4^-.H_3PO_4$, $M_r = 351{\cdot}15$, monoclinic, $P2_1$, $a = 9{\cdot}16(1)$, $b = 8{\cdot}90(1)$, $c = 8{\cdot}81(1)$ Å, $\beta = 111{\cdot}38(5)°$, $V = 669(2)$ Å^3, $Z = 2$, $D_m = 1{\cdot}75$, $D_x = 1{\cdot}74$ Mg m^{-3}, λ(Mo $K\alpha$) = 0·7107 Å, $\mu = 0{\cdot}371$ mm^{-1}, $F(000) = 364$, $T = 293(2)$ K, $R = 0{\cdot}030$ for 2945 data with $I \geq 2{\cdot}5\sigma(I)$; imidazolinium dihydrogen orthophosphate, $(C_3H_5N_2^+.H_2PO_4^-)_2$, $M_r = 332{\cdot}15$, monoclinic, $P2_1/c$, $a = 8{\cdot}53(1)$, $b = 12{\cdot}72(1)$, $c = 15{\cdot}93(1)$ Å, $\beta = 126{\cdot}13(5)°$, $V = 1396(4)$ Å^3, $Z = 4$, $D_m = 1{\cdot}59$, $D_x = 1{\cdot}58$ Mg m^{-3}, λ(Mo $K\alpha$) = 0·7107 Å, $\mu = 0{\cdot}344$ mm^{-1}, $F(000) = 688$, $T = 293(2)$ K, $R = 0{\cdot}046$ for 3382 data with $I \geq 2{\cdot}5\sigma(I)$.

Introduction

Crystalline salts were prepared by reaction of orthophosphoric acid with the bases L-histidine and imidazole, and the products were studied by X-ray crystallography in order to look at the structure of N–H···O–P hydrogen bonds that could be expected to form in the salt crystals. Such hydrogen bonds are of interest because of their widespread biological occurrence. For example, hydrogen bonds between phosphate groups and histidyl imidazolyl groups are involved in the active-site substrate-binding mechanism of ribonuclease (Richards, Wyckoff, Carlson, Allewell, Lee & Mitsui, 1972), and in the regulation of the oxygen affinity of deoxyhemoglobin by 2,3-diphosphoglycerate (Perutz & Ten Eyck, 1972).

The salt crystals prepared in this study have interesting and surprising crystal structures. The imidazolium phosphate salt, which has 1:1 stoichiometry, $Im.H_3PO_4$, crystallized with two chemical formula units in the crystal chemical unit, $(ImH^+.H_2PO_4^-)_2$. The histidinium phosphate salt, which has 1:2 stoichiometry, $His.2H_3PO_4$, was found to be the 1:1 salt co-crystallized with the unionized molecular acid in the crystal chemical unit, $HisH^+.H_2PO_4^-.H_3PO_4$. In both crystal structures the N–H···O and O–H···O hydrogen bonds are very strong, and they form intricate three-dimensional networks. Thermal-vibration analyses indicate that for the phosphate group a rigid-body libration model

0108-7681/86/060613-09$01.50

is not as good as a riding model, with the O-atom vibrations apparently restricted by the hydrogen bonding.

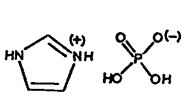

$ImH^+.H_2PO_4^-$

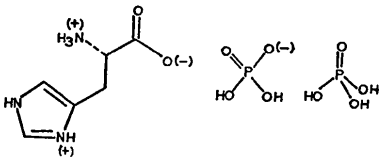

L-$HisH^+.H_2PO_4^-.H_3PO_4$

Experimental work

Crystal syntheses

$(ImH^+.H_2PO_4^-)_2$ was prepared from a solution of 68 mg (1 mmol) imidazole and 70 μl concentrated (85%, relative density 1·7) orthophosphoric acid (1 mmol H_3PO_4) in 30 μl water. $HisH^+.H_2PO_4^-.H_3PO_4$ was prepared from 155 mg (1 mmol) L-histidine and 140 μl phosphoric acid (2 mmol H_3PO_4) in 500 μl water. The product salts crystallized on evaporation of each of these solutions in an evacuated desiccator over anhydrous calcium sulfate. Well formed crystals of the Im salt grew suspended in their very viscous mother liquor after the surface crust of crystals that formed initially was broken up with a glass stirring rod. The crystals of the His salt obtained initially by evaporation were thin laths, but very well formed crystals of stout habit were obtained by vapor diffusion absorption of ethanol into a solution of 1 mmol of the salt in 1·25 ml 1*M* phosphoric acid. Crystals of the Im salt were hygroscopic and eventually deliquesced on standing in air. The crystals of the His salt appeared to be air-stable indefinitely.

Crystallographic measurements

Crystal quality, diffraction symmetry and approximate lattice parameters were determined from sets of Buerger precession photographs. Densities were measured by flotation of the Im crystals in mixed carbon tetrachloride and bromobenzene, and of the His crystals in carbon tetrachloride and methyl iodide. Diffraction intensity data were measured on a Picker FACS-I diffractometer equipped with a Picker–Furnas monochromator device and a pyrolytic graphite monochromator crystal.

The Im specimen crystal had [201]-elongated prismatic habit with prominent {010} and {$\bar{1}$02} prism faces and small {100} end faces; it measured 0·30 × 0·45 × 0·75 mm with its extreme dimensions parallel to [010] and [201]. It was coated with fast-curing epoxy cement to protect it from atmospheric moisture, and mounted with its a^* axis approximately along the goniostat φ axis. The His specimen crystal had *b*-elongated prismatic habit with {100} prominent among the prism faces; it measured 0·33 × 0·87 × 0·60 mm along a^*, *b* and *c*, respectively. It was mounted with its a^* axis approximately along the φ axis.

Lattice parameters were calculated from manually optimized diffractometer setting angles for reflections with $2\theta \simeq 30°$. Reflection intensities were measured as $\theta/2\theta$ scans. All the unique reflections were measured to $(\sin\theta_{max})/\lambda = 0{\cdot}703$ Å^{-1} in the spherical quadrant $-10 \le h \le 9$, $0 \le k \le 17$, $0 \le l \le 22$ for the Im crystal; and $(\sin\theta_{max})/\lambda = 0{\cdot}807$ Å^{-1}, $0 \le h \le 14$, $0 \le k \le 13$, $-13 \le l \le 13$ for the His crystal. In addition, full spheres of low-order reflections $\pm h$, $\pm k$, $\pm l$ were measured for $(\sin\theta)/\lambda \le 0{\cdot}305$ Å^{-1} for the Im crystal, and 0·364 Å^{-1} for the His crystal. For the Im crystal $\bar{5}00$, $0\bar{8}0$ and $30\bar{1}0$ and for the His crystal 400, 800 and 040 were measured at 25-reflection intervals as standard reference reflections. The reference reflections varied by at most ±2·5%, and the data were corrected accordingly using a polynomial interpolation function for the time-dependent scaling. Absorption corrections were not applied. For the Im crystal, 6055 reflections were measured; of these 3824 were unique, and of these 3382 had $I \ge 2{\cdot}5\sigma(I)$, with $\sigma(I)$ based on counting statistics alone. For the His crystal, 5228 reflections were measured, 3098 were unique, and 2945 had $I \ge 2{\cdot}5\sigma(I)$. For the averaging of repeated and equivalent measurements, both data sets gave values of R_{int} of about 3%.

Structure analyses

The His crystal structure was determined by direct methods using symbolic addition, and the Im crystal structure was determined by Patterson and Fourier synthesis techniques based on the P-atom peaks in the Harker line and section. The structure models were refined by least-squares minimization of $\sum w\Delta^2 = \sum w(|F_o| - |F_c|/K)^2$ with $w = (a + |F_o| + c|F_o|^2)^{-1}$ for the reflections with $I \ge 2{\cdot}5\sigma(I)$, and $w = 0$ otherwise. The weighting coefficients had values $a = 2|F_o|_{min} = 20$, $c = 2/|F_o|_{max} = 0{\cdot}0024$ for the Im structure; and $a = 27$, $c = 0.0014$ for the His structure. For both structures, an empirical extinction correction, $|F_o|_{corr} = |F_o|(1 + gI_c)$, was applied before the final cycles of refinement. The extinction correction coefficients, *g*, were obtained from plots of $|F_c|/(K|F_o|)$ *versus* $I_c = \mathrm{Lp}|F_c|^2$ for the 25 reflections in each data set with the largest $|F_c|$. For the Im structure, $g = 2{\cdot}3 \times 10^{-6}$ and $(|F_o|_{corr}/|F_o|)_{max} = 1{\cdot}31$ for the 022 reflection; for the His structure, $g = 1{\cdot}04 \times 10^{-5}$ and $(|F_o|_{corr}/|F_o|)_{max} = 1{\cdot}50$ for the 021 reflection. At intermediate stages of the refinements, all the H atoms were located in difference electron density maps. Anisotropic thermal vibration parameters were refined for the non-H atoms, and isotropic parameters for the H atoms. Neutral free-atom scattering factors (*International Tables for X-ray Crystallography*, 1962) for the non-H atoms, and the contracted spherical-atom approximation for the scattering factor of a bonded H atom (Stewart, Davidson & Simpson, 1965) were used. Computer programs were from the Univer-

sity of Pittsburgh crystallographic program library maintained by Professor R. Shiono. The structure drawings were prepared using the *ORTEP* program (Johnson, 1971).

Final values of the refinement indices are $R = 0{\cdot}030$, $wR = 0{\cdot}043$ and $S = 0{\cdot}39$ for the His structure, and $R = 0{\cdot}046$, $wR = 0{\cdot}074$ and $S = 0{\cdot}47$ for the Im structure. The values of $S < 1$ indicate that the reciprocal weights w^{-1} given by the relative weighting schemes overestimated the observational variances $\sigma^2(|F_o|)$. Values of $\langle w\Delta^2 \rangle$ averaged over intervals of $(\sin\theta)/\lambda$ and $|F|$ magnitude were roughly constant, but larger for the lowest θ, largest $|F|$ reflections. Extreme values in the final difference electron density maps were $(\Delta\rho)_{\min} = -0{\cdot}39$ and $(\Delta\rho)_{\max} = +0{\cdot}68$ e Å^{-3} for the His structure, and $-0{\cdot}43$ and $+0{\cdot}83$ e Å^{-3} for the Im structure. Most of the prominent peaks in the difference density maps occurred between bonded pairs of atoms. The largest shift-to-e.s.d. ratios in the final refinement cycles were for H-atom parameters, with $(\delta/\sigma)_{\max} = 0{\cdot}99$ for the His structure and 0·86 for the Im structure. For the non-H atoms, $\delta/\sigma < 0{\cdot}5$ for both structures. Final atomic parameters are listed in Tables 1 and 2.*

Table 1. *Atomic coordinates and equivalent isotropic mean-square vibrational displacements for* $(Im H^+.H_2PO_4^-)_2$

$$\langle u^2 \rangle_{\text{iso}} = (6\pi^2)^{-1} \sum_{i=1}^{3} \sum_{j=1}^{3} (\mathbf{a}_i \cdot \mathbf{a}_j) b_{ij}, \text{ for } F(\mathbf{h}) = F_0(\mathbf{h}) \exp\left(-\sum_{i=1}^{3} \sum_{j=1}^{3} h_i h_j b_{ij}\right).$$

	x	y	z	$\langle u^2 \rangle_{\text{iso}}$ (Å^2)
N11	0·1875 (3)	0·43783 (16)	0·44154 (15)	0·0470 (8)
C12	0·3483 (4)	0·42930 (21)	0·53670 (20)	0·0529 (10)
N13	0·3822 (3)	0·52045 (18)	0·58475 (16)	0·0518 (9)
C14	0·2392 (4)	0·58884 (20)	0·51942 (22)	0·0580 (12)
C15	0·1154 (4)	0·53775 (21)	0·42884 (20)	0·0519 (10)
N21	−0·3167 (3)	0·03338 (15)	0·47822 (18)	0·0507 (9)
C22	−0·2740 (3)	0·06870 (19)	0·56708 (19)	0·0453 (9)
N23	−0·3815 (3)	0·15260 (14)	0·54893 (14)	0·0412 (7)
C24	−0·4980 (4)	0·17095 (19)	0·44386 (19)	0·0519 (10)
C25	−0·4559 (4)	0·09729 (20)	0·39981 (19)	0·0547 (11)
P1	0·24964 (7)	0·34331 (4)	0·16910 (4)	0·0294 (2)
O11	0·20857 (25)	0·35267 (13)	0·06378 (12)	0·0455 (7)
O12	0·2796 (3)	0·44474 (14)	0·22420 (15)	0·0617 (9)
O13	0·0780 (3)	0·28072 (18)	0·15390 (15)	0·0695 (10)
O14	0·43100 (4)	0·27512 (24)	0·24297 (18)	0·0978 (13)
P2	−0·11424 (7)	0·20832 (4)	0·29686 (4)	0·0283 (2)
O21	0·03128 (23)	0·27930 (13)	0·30052 (12)	0·0435 (6)
O22	−0·32212 (21)	0·22915 (13)	0·20687 (11)	0·0389 (6)
O23	−0·10384 (24)	0·22087 (15)	0·39739 (12)	0·0469 (7)
O24	−0·05461 (24)	0·09264 (13)	0·29403 (14)	0·0498 (7)
HN11	0·134 (6)	0·381 (3)	0·395 (3)	0·081 (12)
HC12	0·438 (6)	0·367 (3)	0·571 (3)	0·083 (13)
HN13	0·498 (6)	0·535 (3)	0·660 (3)	0·075 (12)
HC14	0·232 (5)	0·6659 (25)	0·535 (3)	0·054 (9)
HC15	0·005 (5)	0·564 (3)	0·361 (3)	0·076 (11)
HN21	−0·270 (5)	−0·0245 (25)	0·473 (3)	0·057 (9)
HC22	−0·183 (5)	0·032 (3)	0·636 (3)	0·067 (10)
HN23	−0·370 (4)	0·1912 (21)	0·5987 (21)	0·035 (7)
HC24	−0·583 (4)	0·2273 (21)	0·4134 (22)	0·034 (7)
HC25	−0·524 (6)	0·075 (3)	0·320 (3)	0·075 (12)
HO13	0·087 (5)	0·277 (3)	0·212 (3)	0·068 (10)
HO14	0·516 (7)	0·271 (4)	0·227 (3)	0·104 (15)
HO23	−0·008 (5)	0·2056 (24)	0·446 (3)	0·049 (9)
HO24	−0·134 (6)	0·051 (3)	0·284 (3)	0·073 (11)

Results and discussion

The crystal structures

The $(ImH^+.H_2PO_4^-)_2$ crystal structure is illustrated in Fig. 1, viewed along the direction of its twofold screw axes. This diagram also shows the outlines of both the standard $P2_1/c$ unit cell, which was used in the structure analysis, and the alternative $P2_1/n$ unit cell based on lattice translation vectors **a**, **b** and $\mathbf{c}' = \mathbf{a} + \mathbf{c}$. (This alternative reduced cell was unfortunately not considered until after the structure refinement had been completed; however, even though the excessively oblique interaxial angle β caused correlations between the x and z atomic coordinates to be larger than necessary, no correlation coefficients were larger than 0·6.) As shown in Fig. 1, the Im structure appears to be a layered structure with layers of imidazolium cations at $z = 0$ and $\frac{1}{2}$ alternating between layers of phosphate anions at $z = \frac{1}{4}$ and $\frac{3}{4}$. The imidazolium cations are linked by salt-bridge hydrogen bonds to the adjacent phosphate layers, and the phosphate anions are hydrogen bonded to one another both within and between the phosphate layers.

A quite different impression of the structural organization is given by Fig. 2, which shows two parallel perspectives perpendicular to the direction of the twofold screw axes. These views show that the structure consists of a three-dimensional network of hydrogen-bonded phosphate anions, arranged such that two different kinds of channels through the phosphate network are created. These channels are filled by stacks of the imidazolium cations, hydrogen bonded to the surrounding phosphate anions. In the narrower channels (Fig. 2*a*) the cation stacks are zig-zag; in the broader channels (Fig. 2*b*) they are straight. The stacking interactions between the imidazolium rings have been described in a preliminary structure report (Blessing & McGandy, 1972). The atom numbering and the cation and anion molecular structures, thermal vibrations, and immediate hydrogen-bonded surroundings are illustrated in Fig. 3. It is not obvious why the crystal structure should be as complex as it is, with two chemical formula units in the crystal chemical unit. There are not, for example, any more-or-less discrete dimers of cation–anion pairs. The solution that deposited the crystals contained less than 10% water, so the crystal structure may indicate that phosphate anions encage imidazolium cations in the saturated salt solution.

The $HisH^+.H_2PO_4^-.H_3PO_4$ crystal structure is illustrated in Fig. 4, viewed in projection along the direction of its twofold screw axes. The organization of

* Lists of anisotropic thermal parameters, observed and calculated structure-factor magnitudes and rigid-body thermal vibration tensors have been deposited with the British Library Document Supply Centre as Supplementary Publication No. SUP 43112 (20 pp.). Copies may be obtained through The Executive Secretary, International Union of Crystallography, 5 Abbey Square, Chester CH1 2HU, England.

Table 2. *Atomic coordinates and equivalent isotropic mean-square vibrational displacements for* L-*His*$H^+.H_2PO_4^-.H_3PO_4$

$$\langle u^2\rangle_{iso} = (6\pi^2)^{-1} \sum_{i=1}^{3}\sum_{j=1}^{3} (\mathbf{a}_i.\mathbf{a}_j) b_{ij}, \text{ for } F(\mathbf{h}) = F_0(\mathbf{h}) \exp\left(-\sum_{i=1}^{3}\sum_{j=1}^{3} h_i h_j b_{ij}\right).$$

	x	y	z	$\langle u^2\rangle_{iso}$ (Å^2)
$N^{\delta 1}$	−0·12939 (21)	0·03620 (19)	0·08554 (17)	0·0273 (4)
$C^{\varepsilon 1}$	−0·2035 (3)	0·0422 (3)	−0·07569 (22)	0·0314 (5)
$N^{\varepsilon 2}$	−0·20363 (20)	0·18267 (23)	−0·12249 (18)	0·0304 (4)
$C^{\delta 2}$	−0·12951 (22)	0·27084 (22)	0·01116 (21)	0·0276 (5)
C^{γ}	−0·08129 (19)	0·17905 (19)	0·14411 (18)	0·0208 (4)
C^{β}	0·00482 (19)	0·21097 (22)	0·32058 (18)	0·0227 (4)
N	−0·21191 (16)	0·33684 (19)	0·37707 (16)	0·0230 (4)
C^{α}	−0·10064 (17)	0·20856 (19)	0·42200 (17)	0·0188 (3)
C′	−0·00007 (18)	0·22202 (20)	0·60430 (17)	0·0200 (4)
O″	0·06418 (17)	0·10395 (18)	0·67512 (15)	0·0294 (4)
O′	0·00933 (23)	0·34762 (19)	0·66596 (19)	0·0381 (5)
P1	0·40656 (5)	0·11000	0·00890 (4)	0·01927 (10)
O11	0·49680 (16)	0·12255 (18)	0·18999 (14)	0·0267 (3)
O12	0·45617 (24)	0·22450 (21)	−0·09057 (18)	0·0435 (6)
O14	0·23049 (17)	0·13302 (23)	−0·02044 (17)	0·0365 (5)
O13	0·42421 (21)	−0·04629 (18)	−0·05942 (17)	0·0345 (4)
P2	0·44937 (5)	0·30455 (6)	0·52845 (4)	0·02104 (10)
O21	0·62353 (14)	0·31132 (22)	0·58543 (15)	0·0292 (4)
O22	0·36633 (17)	0·28623 (22)	0·34234 (15)	0·0335 (4)
O23	0·39090 (24)	0·17065 (23)	0·60477 (19)	0·0435 (6)
O24	0·37323 (19)	0·44946 (23)	0·56195 (20)	0·0387 (5)
$H^{\delta 1}$	−0·102 (6)	−0·053 (7)	0·190 (5)	0·090 (15)
$H^{\varepsilon 1}$	−0·251 (3)	−0·033 (4)	−0·150 (4)	0·034 (8)
$H^{\varepsilon 2}$	−0·248 (4)	0·213 (4)	−0·232 (4)	0·040 (9)
$H^{\delta 2}$	−0·124 (5)	0·371 (6)	−0·008 (5)	0·063 (12)
$H^{\beta 2}$	0·093 (4)	0·126 (4)	0·381 (4)	0·031 (7)
$H^{\beta 1}$	0·050 (3)	0·315 (4)	0·333 (4)	0·026 (6)
H1	−0·263 (4)	0·345 (5)	0·451 (4)	0·041 (9)
H3	−0·279 (3)	0·326 (4)	0·277 (3)	0·026 (6)
H2	−0·162 (4)	0·433 (4)	0·385 (4)	0·032 (7)
H^{α}	−0·161 (3)	0·119 (3)	0·401 (3)	0·019 (5)
H14	0·177 (4)	0·137 (5)	−0·125 (4)	0·040 (10)
H13	0·476 (4)	−0·129 (4)	−0·002 (4)	0·047 (8)
H22	0·402 (5)	0·231 (7)	0·307 (5)	0·045 (13)
H23	0·410 (5)	0·186 (5)	0·711 (5)	0·060 (12)
H24	0·404 (6)	0·482 (7)	0·647 (6)	0·097 (17)

this structure is easier to see than that of the imidazolium phosphate structure. The histidinium cations form infinite hydrogen-bonded ribbons along the screw axes at $[0, y, \frac{1}{2}]$, and neighboring ribbons in van der Waals contact form cation layers at $x = 0$.

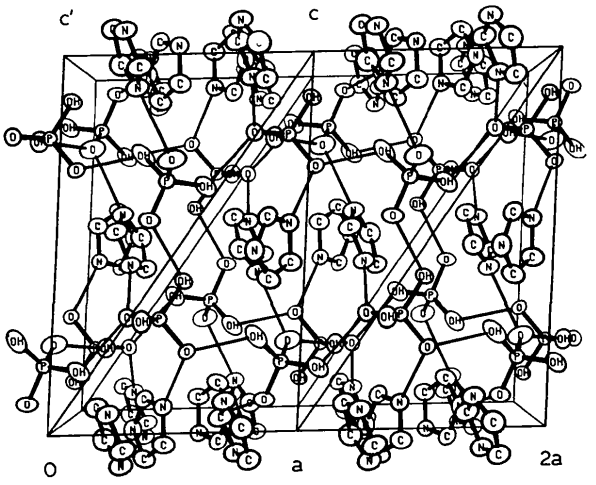

Fig. 1. Perspective drawing of the $(ImH^+.H_2PO_4^-)_2$ crystal structure viewed parallel to the b axis. The very oblique unit cell is the $P2_1/c$ cell used in the structure analysis. The more nearly rectangular cell is the alternative $P2_1/n$ reduced cell based on lattice vectors **a**, **b** and **c**′ = (**a**+**c**) with $c' = 12{\cdot}90$ Å and $\beta' = 93{\cdot}80°$.

The phosphate anions and phosphoric acid molecules form hydrogen-bonded layers at $x = \frac{1}{2}$, with the anions forming infinite hydrogen-bonded chains along the screw axes at $[\frac{1}{2}, y, 0]$, and the molecules arranged along the screw axes at $[\frac{1}{2}, y, \frac{1}{2}]$. The molecules are not hydrogen bonded to one another, but they form hydrogen-bonded cross links between adjacent cation ribbons and between the cation ribbons and anion chains, as well as between neighboring anion chains. The immediate hydrogen-bonded surroundings of the cation, anion and molecule are illustrated along with the molecular structures and thermal vibrations and atom numbering in Fig. 5. Formulation of the crystals

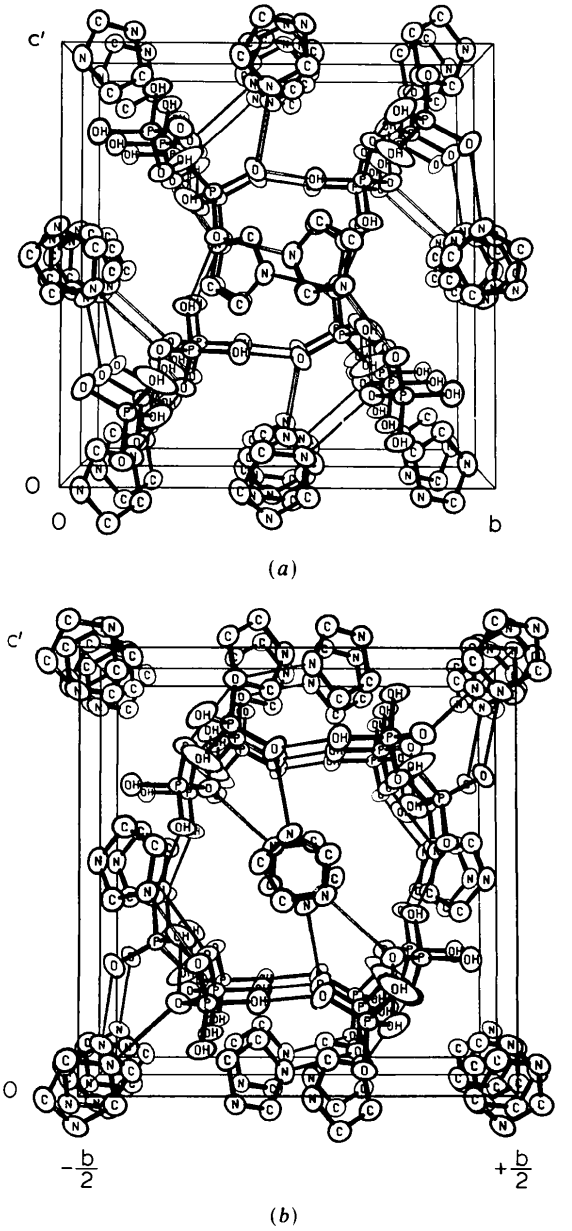

Fig. 2. Perspective drawing of the $(ImH^+.H_2PO_4^-)_2$ crystal structure viewed (*a*) along $[x, \frac{1}{2}, \frac{1}{2}]$ and (*b*) along $[x, 0, \frac{1}{2}]$. In each diagram, the contents of two $P2_1/n$ unit cells (see also Fig. 1) are shown.

as the 1:1 salt co-crystallized with the unionized acid, rather than as a 1:2 salt, $HisH_2^{2+}.2H_2PO_4^-$, is unambiguous, based on molecular geometries and on the refined H-atom positions. It is also consistent with the pK_a values in dilute aqueous solution. For the histidinium dication, $pK_1 = 1{\cdot}8$ ($-CO_2H$), $pK_2 = 6{\cdot}0$ ($-ImH^+$) and $pK_3 = 9{\cdot}3$ ($-NH_3^+$), and so H_3PO_4 with $pK_1 = 2{\cdot}1$ should be a strong enough acid to protonate the imidazolyl group of the histidine zwitterion, but not the carboxylate group.

The L-histidinium monocation has a fully extended *trans* $C'-C^\alpha-C^\beta-C^\gamma$ conformation. This is in contrast to the bent *gauche* conformation in crystals of L-$HisH^+.Cl^-.H_2O$ (Donohue, Lavine & Rollett, 1956; Donohue & Caron, 1964; Hohlwein, 1977), but similar to the *trans* conformation in crystals of DL-$HisH^+.Cl^-.2H_2O$, in which hydrogen-bonded ribbons of histidinium cations, similar to those found in the present study, are also formed (Bennett, Davidson, Harding & Morelle, 1970). In two crystalline forms of L-histidine, the $C'-C^\alpha-C^\beta-C^\gamma$ conformation is also *trans*, but the imidazolyl group is rotated to accept an intramolecular hydrogen bond from the ammonium group to the imidazolyl $N^{\delta 1}$ atom, which is not protonated in the zwitterion free-base structure (Madden, McGandy & Seeman, 1972; Madden, McGandy, Seeman, Harding & Hoy, 1972).

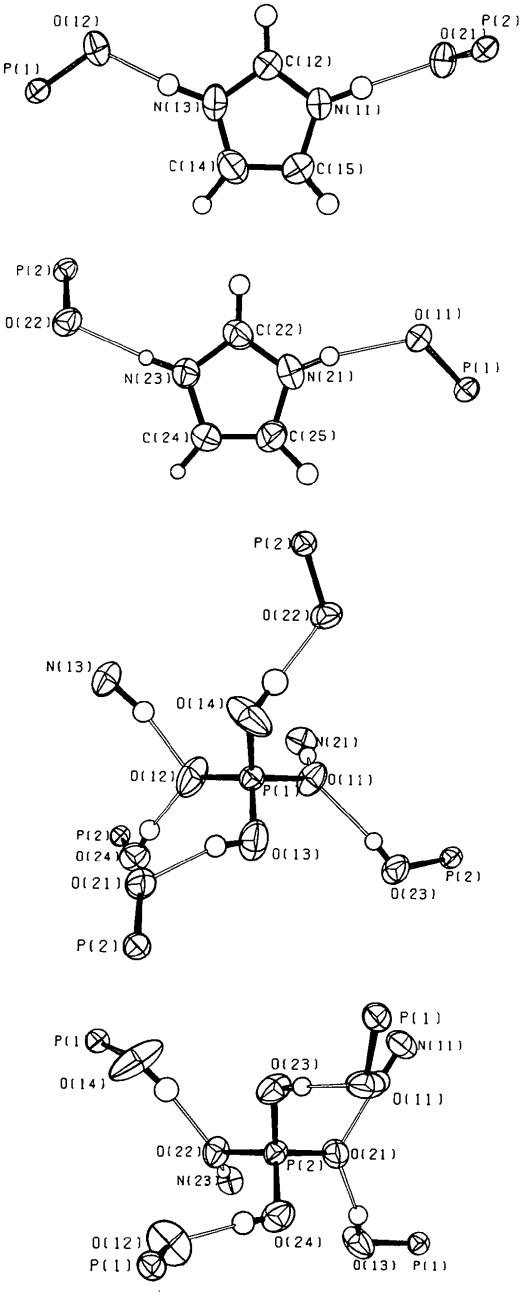

Fig. 3. Atom numbering, molecular structure and thermal vibrations, and immediate hydrogen-bonded surroundings for each of the cations and anions in the $(ImH^+.H_2PO_4^-)_2$ crystal structure. Thermal ellipsoids are 50% equiprobability surfaces for the non-H atoms. The isotropic root-mean-square vibration amplitudes for the H atoms were reduced by a factor of $\frac{1}{2}$ for illustration purposes.

The hydrogen bonding

Both crystal structures contain short strong N–H···O–P and P–O–H···O–P hydrogen bonds (Table 3 and Figs. 3 and 5). The range of N···O distances

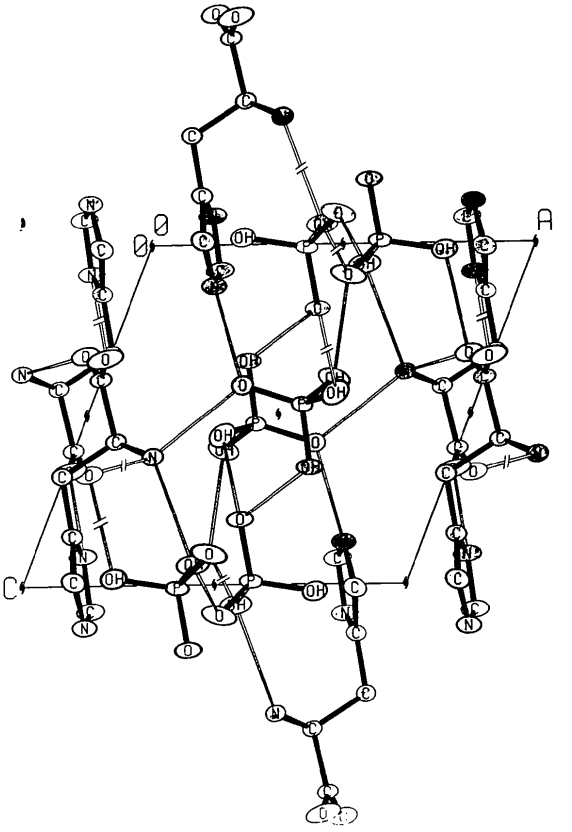

Fig. 4. The L-$HisH^+.H_2PO_4^-.H_3PO_4$ unit cell projected along the *b* axis.

is quite narrow, 2·70–2·72 Å, in the Im structure; it is considerably broader, 2·73–2·95 Å, in the His structure because there are two types of N–H donors, *viz* weaker ammonium $-\overset{+}{N}H_3$ donors as well as stronger iminium $\geqslant\overset{+}{N}$–H donors. The range of O···O distances, 2·56–2·59 Å, is quite narrow in both structures, except for the very short 2·46 Å bond P1–O13–H···O12–P1 that links the phosphate anions into chains in the His structure. Sometimes, O–H···O bonds this short are symmetrical or disordered, with the H atom in a broad shallow potential centered midway between the O atoms or in a double-minimum potential, but the difference electron density quite clearly showed only a single H-atom position in this case.

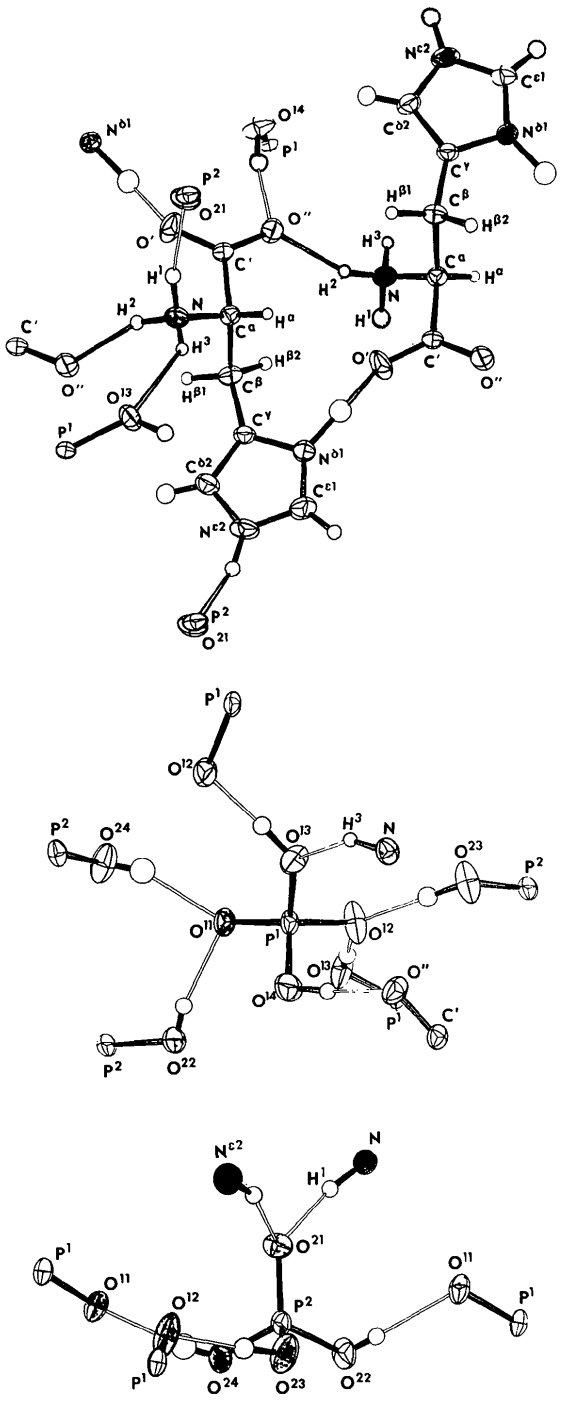

Fig. 5. Atom numbering, molecular structure and thermal vibrations, and immediate hydrogen-bonded surroundings for the cation, anion and molecule in the $HisH^+.H_2PO_4^-.H_3PO_4$ crystal structure. Thermal-vibration amplitudes represented as in Fig. 3.

Table 3. *Hydrogen-bond distances* (Å) *and angles* (°) *in the two crystal structures*

E.s.d.'s are 0·002 to 0·003 Å for *D*···*A*, 0·03 to 0·05 Å for *D*–H and H···*A* and 3 to 5° for *D*–H···*A*. Values in parentheses are normalized to 1·03 Å N–H (Taylor & Kennard, 1984) or 0·97 Å O–H (Jeffrey & Mitra, 1983).

	N···O	N–H	H···O	N–H···O
$(ImH^+.H_2PO_4^-)_2$				
N21–H···O11–P	2·704	0·87 (1·03)	1·85 (1·68)	170 (168)
N23 O22	2·710	0·89 (1·03)	1·83 (1·68)	175 (174)
N11 O21	2·713	0·94 (1·03)	1·78 (1·68)	176 (177)
N13 O12	2·724	1·03 (1·03)	1·71 (1·71)	168 (168)
$HisH^+.H_2PO_4^-.H_3PO_4$				
$N^{\varepsilon 2}$–H···O21–P	2·733	0·94 (1·03)	1·83 (1·75)	160 (159)
N O21	2·777	0·94 (1·03)	1·86 (1·77)	166 (165)
N O13	2·954	0·88 (1·03)	2·21 (2·09)	143 (140)
$N^{\delta 1}$–H···O′–C′	2·658	1·17 (1·03)	1·53 (1·66)	160 (162)
N O″	2·854	0·96 (1·03)	1·94 (1·87)	159 (158)
	O···O	O–H	H···O	O–H···O
$(ImH^+.H_2PO_4^-)_2$				
P–O14–H···O22–P	2·557	0·90 (0·97)	1·68 (1·61)	164 (164)
O24 O12	2·580	0·80 (0·97)	1·79 (1·62)	171 (169)
O23 O11	2·583	0·75 (0·97)	1·84 (1·62)	171 (169)
O13 O21	2·591	0·88 (0·97)	1·74 (1·65)	162 (162)
$HisH^+.H_2PO_4^-.H_3PO_4$				
P–O13–H···O12–P	2·460	0·92 (0·97)	1·54 (1·49)	173 (173)
O22 O11	2·554	0·72 (0·97)	1·85 (1·60)	168 (166)
O23 O12	2·573	0·90 (0·97)	1·68 (1·60)	176 (175)
O24 O11	2·583	0·76 (0·97)	1·87 (1·68)	157 (154)
P–O14–H···O″–C′	2·569	0·87 (0·97)	1·72 (1·62)	167 (167)

The His structure also contains N–H···O–C and P–O–H···O–C bonds to the carboxylate O atoms (Table 3 and Fig. 5). The $N^{\delta 1}$–H···O′–C′ bond that links the histidinium cations together into ribbons is unusually short, with N···O 2·66 Å. This close contact, and the tight hydrogen bonding in the phosphate anion chains in the His structure, contribute to the His crystals being ~10% denser than the Im crystals, even though the Im crystals contain a slightly larger weight percentage of heavy P atoms.

Both structures contain equal numbers of potential hydrogen-bond donors and acceptors: four NH and four OH donors and eight O or OH acceptors in the Im structure; five NH, five OH, and ten O or OH in the His structure. All of the NH and OH groups do function as donors, but only one OH functions as an acceptor – and then only weakly, in the N–H3···O13–P bond, N···O 2·95 Å, in the His structure. In both structures, all of the oxo-type phosphate O atoms are double acceptors. One of the carboxylate O atoms in the His structure is a double acceptor; the other is a single acceptor in the very strong N–H···O bond between histidinium cations.

Table 4. *Bond lengths* (Å) *and valence angles* (°) *in the phosphate groups in the two crystal structures*

Bond-length e.s.d.'s are 0·002 to 0·003 Å for the Im structure and 0·0015 to 0·002 Å for the His structure. Valence-angle e.s.d.'s are 0·1 to 0·15°.

	Uncorrected	Riding model	Rigid-body libration
$(ImH^+.H_2PO_4^-)_2$			
P1–O12	1·495	1·526	1·522
O11	1·503	1·516	1·518
O14H	1·544	1·597	1·572
O13H	1·555	1·583	1·586
P2–O22	1·507	1·517	1·517
O21	1·508	1·520	1·520
O23H	1·559	1·574	1·571
O24H	1·566	1·581	1·580
$HisH^+.H_2PO_4^-.H_2PO_4^-$			
P1–O11	1·510	1·517	1·516
O12	1·518	1·539	1·532
O13H	1·547	1·562	1·560
O14H	1·551	1·567	1·566
P2–O21	1·489	1·496	1·499
O22H	1·544	1·556	1·552
O24H	1·545	1·562	1·557
O23H	1·556	1·576	1·570

	$(ImH^+.H_2PO_4^-)_2$		$HisH^+.H_2PO_4^-.H_3PO_4$	
	$H_2P1O_4^-$	$H_2P2O_4^-$	$H_2PO_4^-$	H_3PO_4
O1–P–O2	115·7	114·3	113·4	114·5
O3	106·8	110·6	112·5	112·4
O4	111·4	106·8	107·6	113·9
O2–P–O3	110·7	106·3	106·6	105·3
O4	106·8	111·0	109·1	102·1
O3–P–O4	105·0	107·6	107·7	107·8

Table 5. *Bond lengths* (Å) *and valence and conformation angles* (°) *in the histidinium and imidazolium cations in the two crystal structures*

E.s.d.'s are 0·003 and 0·004 Å and 0·15 and 0·25° in the His and Im structures, respectively. Libration corrections would add 0·001 to 0·003 Å to the bond lengths in the histidinium cation.

$HisH^+.H_2PO_4^-.H_3PO_4$				$(ImH^+.H_2PO_4^-)_2$		
					Im1	Im2
$N–C^\alpha$	1·485	$C^\alpha–C^\beta$	1·537			
$C^\alpha–C'$	1·537	$C^\beta–C^\gamma$	1·492			
C′–O′	1·232	$C^\gamma–N^{\delta1}$	1·382	C5–N1	1·374	1·372
C′–O″	1·254	$N^{\delta1}–C^{\varepsilon1}$	1·333	N1–C2	1·319	1·315
		$C^{\varepsilon1}–N^{\varepsilon2}$	1·316	C2–N3	1·324	1·323
		$N^{\varepsilon2}–C^{\delta2}$	1·371	N3–C4	1·353	1·372
		$C^{\delta2}–C^\gamma$	1·363	C4–C5	1·350	1·340
$N–C^\alpha–C'$	108·1	$C^\alpha–C^\beta–C^\gamma$	113·4			
C^β	110·5	$C^\beta–C^\gamma–N^{\delta1}$	122·7			
$C^\alpha–C'–O'$	116·8	$C^{\delta2}$	131·6			
O″	116·6	$C^\gamma–N^{\delta1}–C^{\varepsilon1}$	109·3	C5–N1–C2	108·5	108·6
O′–C′–O″	126·6	$N^{\delta1}–C^{\varepsilon1}–N^{\varepsilon2}$	108·3	N1–C2–N3	108·5	108·9
		$C^{\varepsilon1}–N^{\varepsilon2}–C^{\delta2}$	109·3	C2–N3–C4	109·1	108·3
		$N^{\varepsilon2}–C^{\delta2}–C^\gamma$	107·4	N3–C4–C5	107·2	107·1
		$C^{\delta2}–C^\gamma–N^{\delta1}$	105·7	C4–C5–N1	106·7	107·0

H1–N–C^α–C′	φ_1	−49
H2	φ_2	+65
H3	φ_3	−172
N–C^α–C′–O′	ψ_1	−21·7
O″	ψ_2	+158·4
N–C^α–C^β–C^γ	χ_1	−68·0
C^α–C^β–C^γ–$N^{\delta1}$	$\chi_{2,1}$	−75·6
$C^{\delta2}$	$\chi_{2,2}$	+104·2

Molecular geometries and thermal-vibration analyses

Bond distances and angles involving non-H atoms are listed in Table 4 for the phosphate groups in the two crystal structures, and in Table 5 for the histidinium and imidazolium cations. The range of C–H bond lengths in the two structures is 0·93 to 1·09 Å; N–H and O–H bond lengths are included with hydrogen-bond distances and angles in Table 3.

Thermal-motion corrections for the P–O bond lengths are discussed below, but with or without the corrections the bond lengths fall into two broad classes, *viz* shorter P=O bonds with formal double-bond character to oxo O atoms, and longer P–OH formal single bonds to hydroxy O atoms. Bond-length variations within these two groups are at least partly attributable to hydrogen-bonding effects on the $p\pi(O) \rightarrow d\pi(P)$ partial double-bond character, according to formal schemes of the type

$$P–O–H\cdots O=P \leftrightarrow P–O–H\cdots \bar{O}–\overset{+}{P}$$

and

$$P–O–H\cdots O–P \leftrightarrow \bar{P}=\overset{+}{O}–H\cdots O–P.$$

For example, in the His crystal structure, the P1–O12 bond is the longest bond to an oxo O atom, and the P1–O13 bond is the shortest bond to a hydroxy O atom (Table 4), and these two are also the acceptor and the donor, respectively, in the shortest hydrogen bond in the structure, P1–O13–H···O12–P1 (Table 3).

The thermal-vibration-amplitude parameters were put to the rigid-bond test (Hirshfeld, 1976), to check the deconvolution of the thermal-vibration displacements from the valence electron density deformations, and to the rigid-molecule test (Rosenfeld, Trueblood & Dunitz, 1978), to check whether low-frequency internal molecular vibration modes were excited along with the external rigid-body lattice-vibration modes. The results, which are summarized in Table 6, showed that the thermal parameters are only moderately accurate. Highly accurate parameters should give $|\Delta\langle u^2\rangle| \leq 0{\cdot}001$ Å^2 along the C–C, C–N and C–O bonds (Hirshfeld, 1976), whereas the present results gave average and maximum values of 0·002 and 0·01 Å^2. This probably means that because

Table 6. *Summary of rigid-bond- and rigid-molecule-test results*

Average and maximum differences (Å^2) in mean-square amplitudes of vibration along bonded and non-bonded intramolecular interatomic directions between non-H atoms.

$A–B$	$\lvert\Delta\langle u^2\rangle\rvert = \lvert\langle u_A^2\rangle - \langle u_B^2\rangle\rvert$ average	maximum	Comment
Phosphate groups			
P–O	0·010	0·035, 0·032	Maxima for O14 and O13 in the Im structure
	0·007	0·014	Excluding O14 and O13
O–O	0·009	0·050	Maximum for O14–O12 in the Im structure
Histidinium and imidazolium cations C–C, C–N, C–O, N–N, N–O, O–O			
His	0·0027	0·010	
Im1	0·0014	0·003	
Im2	0·004	0·010	
C–C, C–N, C–O	0·0021	0·010	Bonded pairs only

the data did not extend beyond $(\sin\theta)/\lambda$ of 0·7 or 0·8 $Å^{-1}$ the thermal parameters refined to values that were slightly too large in bond and lone-pair directions in an attempt to cover the valence-density deformations, a conclusion also supported by the appearance of deformation density features in the final difference maps. It is also possible that crystals as large as those used in these studies might not have been uniformly illuminated in all orientations in the X-ray beam from the crystal monochromator (Fig. 5 in Coppens, Ross, Blessing, Cooper, Larsen, Leipoldt, Rees & Leonard, 1974). This would lead to errors resembling anisotropic absorption errors, which would affect mainly the thermal parameters.

The rigid-molecule-test results were no worse than the rigid-bond-test results, so the independent-atom thermal-vibration parameters U_{ij} were fitted by rigid-body **TLS** models (Schomaker & Trueblood, 1968). Results are summarized in Table 7 for the histidinium cation and for the phosphate groups in the two structures. For the imidazolium cations, **T** and **L** tensors were indeterminate by least-squares fit, because, for these symmetrical planar structures, out-of-plane translational vibrations are formally indistinguishable from librations about in-plane axes (Johnson & Levy, 1974). For the histidinium cation, a rigid-body plus non-rigid librating group **TLS**+Ω model (Dunitz & White, 1973; Trueblood, 1978) was also fitted, which allowed for torsional oscillations of the carboxylate group about the C'–C^α bond and the imidazolium group about the C^γ–C^β bond. The resulting group libration amplitudes were insignificant, $\langle\omega^2\rangle^{1/2} = 0{\cdot}7\,(13)$ and $0{\cdot}0\,(8)°$, respectively, and there was no improvement in the agreement of the fit.

The agreement statistics for the **TLS** models were only moderately good, but the results generally indicated that the atomic displacements were mostly due to translational lattice modes with, coincidently, the three principal vibration directions roughly along the **a**, **b** and **c*** directions, respectively, for both structures (see Figs. 1 and 3). The principal libration axes were reasonably close to the molecular inertial axes for the histidinium cation, but for the phosphate groups in the two structures the libration axes were not rationally oriented with respect to either molecular or crystallographic axes.

Bond-length corrections for the apparent shortening due to the rigid-body librations were only 0·001–0·003 Å for the histidinium cation. Comparison of chemically equivalent bond lengths in the histidyl imidazolium group and the imidazolium cations (Table 5) indicates that the indeterminate librational vibrations of the imidazolium cations shorten the apparent bond lengths by at least 0·01 Å. Libration corrections were also 0·01 Å or more for the phosphate groups, and libration-corrected bond lengths are included in Table 4. Also given in Table 4 are bond lengths corrected according to the riding model (Busing & Levy, 1964), assuming that the phosphate O atoms rigidly follow the (translational) vibrations of the heavier P atom and undergo additional independent vibrations perpendicular to the P–O bonds. The libration model and the riding model gave approximately equal corrections for all except the P1–O14H bond in the Im structure, for which the riding model seemed to over correct. This bond also gave the worst result in the rigid-bond test (Table 6).

Table 7. *Agreement-of-fit indices and root-mean-square principal amplitudes for rigid-body translations* (**T**) *and librations* (**L**)

$R = [\sum \Delta^2/\sum (u_{ij})^2]^{1/2}$, $\Delta = u_{ij}$ (independent atom) $- u_{ij}$(**T**, **L**, **S**).
$wR = [\sum w\Delta^2/\sum w(u_{ij})^2]^{1/2}$, $w = 1/\sigma^2(u_{ij})$.
$\Delta_{r.m.s.} = (\sum \Delta^2/N)^{1/2}$; $\Delta_{r.w.m.s.} = (\sum w\Delta^2/\sum w)^{1/2}$.

	$HisH^+.H_2PO_4^-.H_3PO_4$			$(ImH^+.H_2PO_4^-)_2$	
	$HisH^+$	$H_2PO_4^-$	H_3PO_4	$H_2P1O_4^-$	$H_2P2O_4^-$
R	0·18	0·15	0·15	0·27	0·099
wR	0·18	0·093	0·082	0·16	0·082
$\Delta_{r.m.s}$ (Å²)	0·0038	0·0039	0·0038	0·013	0·0031
$\Delta_{r.w.m.s}$ (Å²)	0·0019	0·0008	0·0009	0·0023	0·0010
$T_1\langle u^2\rangle^{1/2}$ (Å)	0·162	0·178	0·167	0·210	0·200
T_2	0·141	0·132	0·157	0·169	0·178
T_3	0·113	0·102	0·110	0·138	0·132
$L_1\langle\omega^2\rangle^{1/2}$ (°)	3·5	7·1	6·3	10·4	5·9
L_2	2·3	4·2	4·0	6·1	4·9
L_3	1·2	3·0	3·6	4·8	4·1

Qualitatively, the major vibration amplitude for O14 (see Figs. 2 and 3) certainly appears to be anomalously large, but its direction is consistent with the vibrations of the other O atoms in these structures, nearly all of which have their major amplitude in a direction approximately perpendicular to the plane in which they are covalently bound and donate or accept hydrogen bonds (see Figs. 3 and 5). This correlation of thermal-ellipsoid orientations with hydrogen-bonding geometry suggests that the riding model might be more appropriate than the rigid-body model for the phosphate groups. The ellipsoid orientations shown in Figs. 3 and 5 do not reveal obvious patterns of rigid-body libration for the phosphate groups, and the results summarized in Table 6 also indicate that the phosphate groups are non-rigid.

Significance in structural chemistry and biochemistry

The dimensions of the phosphate groups and hydrogen bonds are consistent with the P–OH and O–H···O data recently reviewed by Ferraris & Ivaldi (1984). The P–O distances within the PO_4 tetrahedra vary considerably, while the average P–O distance and the O···O distances along the edges of the tetrahedra remain about constant. Thus, depending on how many of the phosphate O atoms are protonated, the P atom is displaced from the center of the tetrahedron, adjusting the relative amounts of P–O partial double-bond character and the lengths of the P–O bonds, and maintaining a constant average or total P–O bond strength. The present results empha-

size that the relative P–O bond strengths are also strongly influenced by hydrogen bonding, which can stretch and weaken P–O acceptor bonds, and contract and strengthen P–OH donor bonds, by ~0·02 Å. This is a large effect, about a third of the ~0·06 Å change in P–O bond length that accompanies protonation or proton dissociation.

The geometries of N–H···O–C and of C–O–H···O–C hydrogen bonds have been reviewed recently by Taylor & Kennard (1984) and Jeffrey & Mitra (1983), respectively. By comparison, the present results show that N–H···O–P and P–O–H···O–P bonds are considerably stronger than N–H···O–C and C–O–H···O–C bonds, with normalized H···O distances (Table 3) shorter by ~0·2 Å, on average, in the phosphate hydrogen bonds. Indeed, hydrogen bonds involving phosphate groups are probably the strongest N–H···O and O–H···O bonds that form in biochemical systems. They should, therefore, be expected to play important roles in biomolecular structure, energetics and dynamics - especially so in the case of protein-nucleic acid interactions and in the many biochemical reaction mechanisms involving ATP hydrolysis or ADP phosphorylation. In particular, the strong effects of hydrogen bonding and proton transfer on P–O bond strengths are probably important factors for activating reactants and stabilizing intermediates in the reactions of the ATP-ADP biochemical energy cycle.

The experimental work and much of the computational analysis were done in the Department of Crystallography at the University of Pittsburgh while the author was an NIH postdoctoral trainee there during 1970–1972 supported by USPHS grant No. GM-01728. Work done in Buffalo was supported by USDHHS PHS NIH grant Nos. GM-34073 and AM-19856.

References

BENNETT, I., DAVIDSON, A. G. H., HARDING, M. M. & MORELLE, I. (1970). *Acta Cryst.* B**26**, 1722-1729.
BLESSING, R. H. & MCGANDY, E. L. (1972). *J. Am. Chem. Soc.* **94**, 4034-4035.
BUSING, W. R. & LEVY, H. A. (1964). *Acta Cryst.* **17**, 142-146.
COPPENS, P., ROSS, F. K., BLESSING, R. H., COOPER, W. F., LARSEN, F. K., LEIPOLDT, J. G., REES, B. & LEONARD, R. (1974). *J. Appl. Cryst.* 7, 315-319.
DONOHUE, J. & CARON, A. (1964). *Acta Cryst.* **17**, 1178-1180.
DONOHUE, J., LAVINE, L. R. & ROLLETT, J. R. (1956). *Acta Cryst.* **9**, 655-662.
DUNITZ, J. D. & WHITE, D. N. J. (1973). *Acta Cryst.* A**29**, 93-94.
FERRARIS, G. & IVALDI, G. (1984). *Acta Cryst.* B**40**, 1-6.
HIRSHFELD, F. L. (1976). *Acta Cryst.* A**32**, 239-244.
HOHLWEIN, D. (1977). *Acta Cryst.* A**33**, 649-654.
International Tables for X-ray Crystallography (1962). Vol. III, pp. 201 *ff.* Birmingham: Kynoch Press. (Present distributor D. Reidel, Dordrecht.)
JEFFREY, G. A. & MITRA, J. (1983). *Acta Cryst.* B**39**, 469-480.
JOHNSON, C. K. (1971). *ORTEP.* Report ORNL-3794, 2nd revision. Oak Ridge National Laboratory, Tennessee.
JOHNSON, C. K. & LEVY, H. A. (1974). In *International Tables for X-ray Crystallography*, Vol. IV, pp. 311 *ff.* Birmingham: Kynoch Press. (Present distributor D. Reidel, Dordrecht.)
MADDEN, J. J., MCGANDY, E. L. & SEEMAN, N. (1972). *Acta Cryst.* B**28**, 2377-2382.
MADDEN, J. J., MCGANDY, E. L., SEEMAN, N., HARDING, M. M. & HOY, A. (1972). *Acta Cryst.* B**28**, 2382-2389.
PERUTZ, M. F. & TEN EYCK, L. F. (1972). *Cold Spring Harbor Symp. Quant. Biol.* **36**, 295-310.
RICHARDS, M. F., WYCKOFF, H. W., CARLSON, W. D., ALLEWELL, N. M., LEE, M. & MITSUI, Y. (1972). *Cold Spring Harbor Symp. Quant. Biol.* **36**, 25-43.
ROSENFELD, R. E., TRUEBLOOD, K. N. & DUNITZ, J. D. (1978). *Acta Cryst.* A**34**, 828-829.
SCHOMAKER, V. & TRUEBLOOD, K. N. (1968). *Acta Cryst.* B**24**, 63-76.
STEWART, R. F., DAVIDSON, E. R. & SIMPSON, W. T. (1965). *J. Chem. Phys.* **42**, 3175-3187.
TAYLOR, R. & KENNARD, O. (1984). *Acc. Chem. Res.* **17**, 320-326.
TRUEBLOOD, K. N. (1978). *Acta Cryst.* A**34**, 950-954.

Acta Cryst. (1986). B**42**, 621-626

Orientational Disorder in Cyclohepta[*de*]naphthalene. Structure Determination at 78, 100, 135, 200 and 295 K

BY ALAN HAZELL, RITA GRØNBÆK HAZELL AND FINN KREBS LARSEN

Department of Chemistry, Aarhus University, DK-8000 Århus C, Denmark

(*Received* 1 *April* 1986; *accepted* 4 *July* 1986)

Abstract

Cyclohepta[*de*]naphthalene (pleiadiene), $C_{14}H_{10}$, $M_r = 178{\cdot}2$, monoclinic, $P2_1/c$, is disordered at room temperature, the molecules reorientating in their planes. The structure is ordered at 78 K with $a = 8{\cdot}210\ (4)$, $b = 10{\cdot}691\ (5)$, $c = 11{\cdot}034\ (5)$ Å, $\beta = 104{\cdot}75\ (3)°$, $V = 937\ (1)$ Å^3, $Z = 4$, $D_x = 1{\cdot}264\ (1)$ Mg m^{-3}, Mo $K\alpha$, $\lambda = 0{\cdot}71069$ Å, $\mu = 0{\cdot}0675\ (1)$ mm^{-1}, $F(000) = 376$. $R(F) = 0{\cdot}046$ for 976 reflexions [$I > 3\sigma(I)$] and 63 variables. The disorder has been studied by energy calculations and by constrained least-squares refinements with data collected at five temperatures. Four possible orientations were

0108-7681/86/060621-06$01.50